Nanoscience and
Nanotechnology Letters
Vol. 3, 181–185, 2011

Blocking Layer Effect on Dye-Sensitized Solar Cells Assembled with TiO_2 Nanorods Prepared by dc Reactive Magnetron Sputtering

Lijian Meng[1, 2, *] and Can Li[3]

[1] *Departamento de Física, Instituto Superior de Engenharia do Porto, Rua Dr. António Bernardino de Almeida, 431, 4200-072 Porto, Portugal*
[2] *Centro de Física, Universidade do Minho, 4800-058 Guimarães, Portugal*
[3] *State Key Laboratory of Catalysis, Dalian Institute of Chemical Physics, Chinese Academy of Sciences, 457 Zhongshan Road, Dalian 116023, China*

Three different thickness dense TiO_2 (150 nm, 300 nm and 450 nm respectively) films were deposited on ITO substrates by dc reactive magnetron sputtering technique. These dense TiO_2 films were used as the blocking layers. After that, TiO_2 nanorod films were deposited on these dense TiO_2 films by same technique. Both the dense and nanorod TiO_2 films have an anatase phase. The dense TiO_2 films have an orientation along the [101] direction and the TiO_2 nanorod films show a very strong orientation along the [110] direction. These TiO_2 materials were sensitized by N719 dye and the DSSCs were assembled using them as photoelectrode. The effect of the blocking layer on the efficiency of the DSSCs is discussed. The DSSC assembled using TiO_2 nanorod film with 300 nm thickness blocking layer shows a high efficiency of 2.07%.

Keywords: TiO_2, DSSC, Nanorod, Sputtering, Blocking Layer, Solar Cell, Dye-Sensitized.

1. INTRODUCTION

Producing the energy using the fossil materials (petroleum and coal) will pollute the environment. Since Copenhagen Climate Summit in 2009, not only the scientists and politicians, but also more and more common people concerns about the global warming and climate changes. In addition, these fossil materials are becoming depleted very fast. Therefore it is necessary to find a new energy source to replace these traditional sources. For decreasing air pollution and carbon dioxide emission, solar energy has been considered as the most important energy source: it is abundant, clean and safe. Dye-sensitized solar cells (DSSCs) have been attracting a lot of interests because of high energy conversion efficiency and the possibility of low production cost since it has been invented by Gratzel in 1991.[1] The principle of the DSSC is based on the injection of the electrons from the adsorbed dye molecules into the conduction band of the nanocrystalline TiO_2. These electrons are transferred to the external load through the nanocrystalline TiO_2 layer. The dye is regenerated by electron donation from the redox system of the electrolyte, such as the iodide/triiodide couple. The iodide is regenerated by the reduction of triiodide at the platinum layer of the counter electrode.[2] In the DSSC device, nanocrystalline TiO_2 layer plays a very important role. Generally, this nanocrystalline TiO_2 layer is made by chemical methods.[1–8] Although the DSSC devices assembled with nanoporous TiO_2 prepared by chemical methods has achieved conversion efficiency about 11%,[2,8] these chemical methods have some limitations for the industrial production, not only for large area production but also for the reproduction. Sputtering technique is a good technique for the industrial production and has been used for producing the nanocrystalline TiO_2 for DSSC devices.[9–13] However, the conversion efficiency of the DSSC devices assembled with the nanocrystalline TiO_2 prepared by sputtering technique is still low comparing to those by chemical methods. Therefore, more scientific research work is still needed for improving the conversation efficiency.

The nanocrystalline TiO_2 layers used in DSSC devices often contain small holes that allow direct contact between the electrolyte and the conducting electrode and result in the charge leakage. In order to prevent the carriage leakage, a blocking layer has been used between the conducting electrode and the nanocrystalline TiO_2 layer. And

*Author to whom correspondence should be addressed.

some work have been reported by using different type of materials as blocking layers and using different thickness of blocking layers.[14–22] All these work reported the effects of the blocking layers on DSSC devices assembled using nanocrystalline TiO_2 prepared by chemical methods. No reported on the effect of the blocking layers on TiO_2 prepared by sputtering method has been found until now. In our previous work, we have reported the effect of dimension of the TiO_2 nanorod prepared by sputtering technique on DSSC devices.[23] In this work, we report the blocking layer effect on the DSSC devices assembled with TiO_2 nanorods prepared by sputtering technique. The structural, optical and the photovoltaic properties of the DSSC devices with different thickness of the blocking layers prepared by sputtering technique have been studied.

2. EXPERIMENTAL DETAILS

The TiO_2 dense films were prepared on the commercial ITO (sheet resistance of 20 Ω per square and thickness of 100 nm) substrates by dc reactive magnetron sputtering technique using a commercial sputtering system equipped with a turbo molecular pumping system. After that the TiO_2 nanorod films were prepared on these dense TiO_2 films by same system. A titanium metal disk (60 mm in diameter and 3 mm in thickness) with a purity of 99.99% was used as the target. After pumping down to 1×10^{-3} Pa, the oxygen and argon gases (99.99% purities) were introduced into the chamber through the mass flow controllers. For the dense TiO_2 films, the oxygen partial pressure and the total sputtering pressure were 4.5×10^{-2} Pa and 0.3 Pa, respectively. The target-substrate distance was 50 mm. The deposition times were 15, 30 and 45 minutes, respectively. The sputtering was carried out using a constant current mode. The sputtering current was kept at 0.5 A and the sputtering power was about 185 W. In order to remove surface contaminants of the target, pre-sputtering was done for 20 minutes with a shutter covering the substrate. After that, the TiO_2 nanorod films were deposited on these dense TiO_2 films with following conditions: the oxygen partial pressure and the total sputtering pressure were 0.3 Pa and 1.5 Pa, respectively. The target-substrate distance was 50 mm. The deposition time was 180 minutes. The sputtering was carried out using a constant current mode. The sputtering current was kept at 0.5 A and the sputtering power was about 215 W. The transmittance of the films was measured using a Jasco V-550 UV-Vis spectrophotometer. The XRD measurements have been done using Rigaku miniflex goniometer (30 kV, 15 mA). The morphologies of the nanorods were studied using field emission scanning electron microscope (FE-SEM). Raman scattering measurements have been done using a semiconductor laser and a 532 nm laser line is used as exciting light. The laser line is focused on the sample surface in a strict 180° backscattering geometry.

The TiO_2 films were sensitized with N719 (Ru(II)L2(NCS)2:2TBA, where $L = 2, 2'$-bipyridyl-4,4′-dicarboxylic acid) dye by soaking the films in an ethanolic solution of N719 dye (0.5 mM) of for 24 hours at room temperature. The counter-electrode was made by sputtering Pt on an FTO glass and the electrolyte is composed of 0.1 M I_2, 0.1 M LiI, 0.6 M 1-hexyl-3-methylimidazolium iodide, and 0.5 M 4-tert-butylpyridine in 3-methoxypropionitrile. The photocurrent–voltage measurements were carried out with a Princeton 2273 applied research electrochemical system, a 500 W Xenon lamp under AM 1.5 G illumination with a water filter was used. The light intensity was adjusted to 100 mW/cm^2. Cells with an active area of 0.15 cm^2 were tested.

3. RESULTS AND DISCUSSION

SEM analysis showed that the TiO_2 blocking layer has a very compact structure as shown in Figure 1(a). The structures of the TiO_2 nanorods deposited on ITO substrate and on TiO_2 blocking layer are shown in Figures 1(b and c). It can be seen that the TiO_2 nanorods deposited directly on ITO substrate or on TiO_2 blocking layer have the

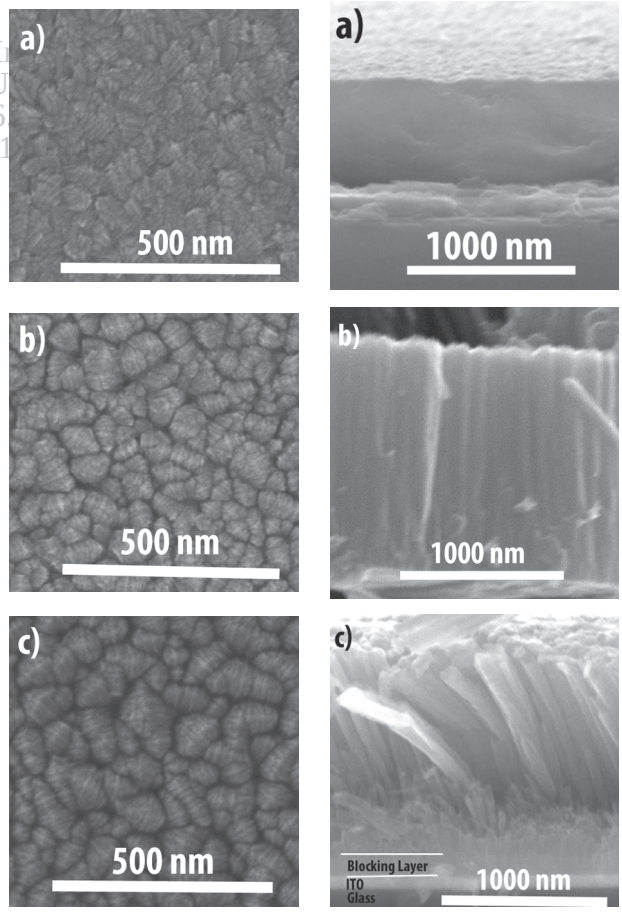

Fig. 1. (a) Dense TiO_2 film on ITO substrate; (b) TiO_2 nanorods on ITO substrate; (c) TiO_2 nanorods on 150 nm thickness dense TiO_2 film.

same structures. It also can be seen from the SEM images that the length of the TiO_2 nanorods are about 1200 nm. Figure 2 shows the XRD patterns of TiO_2 blocking layer deposited on ITO substrate (a), TiO_2 nanorods deposited on ITO substrate (b), and on different thicknesses of TiO_2 blocking layers (c, d, e). Both the TiO_2 blocking layer and the TiO_2 nanorods show only anatase phase, no rutile phase has been observed. Rutile phase has been observed for sputtered TiO_2 blocking layer in some reported work.[14, 21] In those reported work, the substrate were heated and may result in the formation of the rutile phase. In this work, the substrates were not heated and only anatase phase is formed. It can be seen that the TiO_2 blocking layer deposited on ITO substrate has an orientation along the [101] direction and the TiO_2 nanorods deposited on ITO substrate has an orientation along the [110] direction. The TiO_2 nanorods deposited on blocking layers with different thicknesses still have the preferred orientation along the [110] direction. It means that the blocking layer does not modify the orientation and the structure of the TiO_2 nanorods.

The optical transmission spectra of the TiO_2 blocking layer deposited on the glass substrate and the TiO_2 nanorods deposited on the glass and 300 nm thickness blocking layer substrates are given in Figure 3. From the interference fringe it can be concluded that the TiO_2 blocking layer has a high refractive index than TiO_2 nanorods. As it can be seen from the SEM images that the blocking layer has a very compact structure, it means a high packing density and then a high refractive index. And TiO_2 nanorods have many voids between the nanorods, it means a low packing density and then a low refractive index. It can be seen from the transmittance that the optical bandgap has a red shift for TiO_2 nanorod film comparing to the TiO_2 blocking layer. Generally, the bandgap of the nano-structural TiO_2 has a blue shift because of

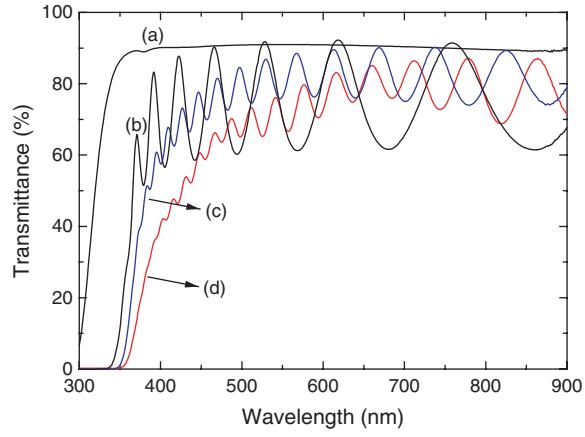

Fig. 3. Transmission spectra: (a) Glass substrate; (b) Blocking layer on glass; (c) TiO_2 nanorods on glass; (d) TiO_2 nanorods on 300 nm thickness blocking layer.

the contribution of quantum size effect.[24, 25] However, the results given in Figure 3 do not agree with these general results. It is suggest that the red shift of the bandgap is mainly due to the difference of the thickness. As it has been well known that the optical bandgap has a red shift as the thickness is increasing. From the SEM images it can be seen that the thickness of the dense TiO_2 film is about 700 nm and the thickness of the TiO_2 nanorod film is about 1200 nm. In addition, it has been reported that a large bandgap can be caused by an axial strain effect from lattice deformation.[26] In this work, the dense TiO_2 blocking layers were deposited at low sputtering pressure, and the TiO_2 nanorod films were deposited at high sputtering pressure. Our previous work[27] has shown that TiO_2 films prepared at high sputtering are subject to a low residual stress and may result in the red shift of the band gap.

Figure 4 shows the Raman spectra of the dense TiO_2 film deposited on ITO substrate and the TiO_2 nanorod

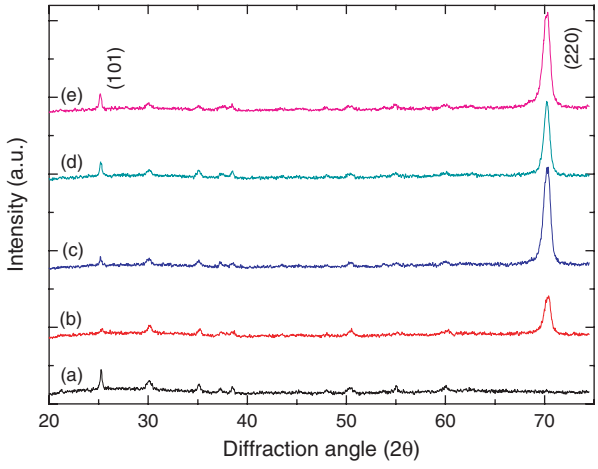

Fig. 2. XRD patterns of different samples. (a) Blocking layer on ITO substrate; (b) TiO_2 nanorods on ITO substrate; (c) TiO_2 nanorods on 150 nm thickness blocking layer; (d) TiO_2 nanorods on 300 nm thickness blocking layer; (e) TiO_2 nanorods on 450 nm thickness blocking layer.

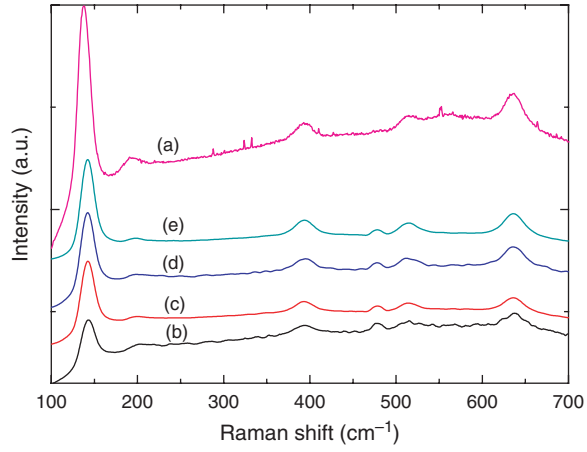

Fig. 4. Raman spectra of different samples: (a) Blocking layer on ITO substrate; (b) TiO_2 nanorod on ITO substrate; (c) TiO_2 nanorod on 150 nm thickness blocking layer; (d) TiO_2 nanorod on 300 nm thickness blocking layer; (e) TiO_2 nanorod on 450 nm thickness blocking layer.

films deposited both on ITO and dense TiO_2 substrates. The five Raman peaks located at 144 cm^{-1}, 197 cm^{-1}, 399 cm^{-1}, 519 cm^{-1} and 639 cm^{-1} can be assigned as the E_g, B_{1g}, A_{1g} or B_{1g}, and E_g modes of the anatase phase respectively. No rutile phase has been observed which is consistent with the XRD measurements as shown in Figure 2. Although the dense TiO_2 film and TiO_2 nanorod film have different growth orientations, Raman is not sensitive to this difference. However, the Raman peak intensity of dense TiO_2 film is much stronger than TiO_2 nanorod films. It means TiO_2 nanorod structure will result in the decrease of the lattice vibration intensity.

Photocurrent–voltage characteristics of DSSCs without and with different thicknesses of blocking layers are compared in Figure 5. Measured solar cell parameters are summarized in Table I. It can be seen from the Table I that the photocurrents of the DSSC devices with 150 nm thickness blocking layer are increased by more than 40%, compared to those of the devices without the blocking layer. In addition, the photocurrent is increased further as the thickness of the blocking layer is increased. Generally, dye loading in TiO_2 photoelectrode and the charge recombination at photoanode are two key influences on the photocurrent of DSSC devices. Although the dye loading amounts are not calculated for these work, from the measurements of the XRD and SEM it can be seen that the structures of these TiO_2 nanorod films are not modified by introducing the blocking layers. It can be suggested that the dye loading amounts will not be influenced by the blocking layer. Therefore, the increase of the photocurrent is mainly due to the improvement of the charge recombination at ITO/electrolyte interfaces. As it can be seen from SEM images that the blocking layer has a very compact structure, the bare ITO recombination places will be reduced by introducing this blocking layer between the ITO substrate and TiO_2 nanorod films. The charge recombination in the DSSC devices is effectively suppressed and results in an increase of the photocurrent. In addition, as the blocking layer has a dense compact structure and also a large contact area with ITO substrate comparing to the nanorod films, more effective electron pathways will be generated via the blocking layer to improve electron transportation. Therefore, more electrons can be collected at the conduction band of the photoanode and transferred to external circuit, resulting in an increase of the photocurrent of the DSSC devices. The possibility of the charge recombination at ITO/electrolyte interfaces will decrease as the thickness of the blocking layer is increased and results in an increase of the photocurrent with the thickness of the blocking layer.

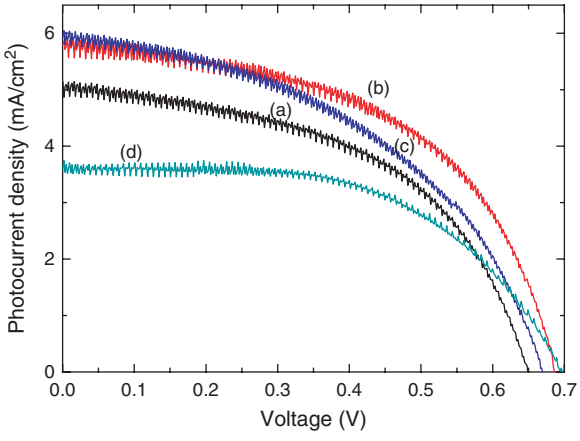

Fig. 5. *J–V* curves: the thickness of the blocking layer is 150 nm, 300 nm and 450 nm for (a), (b) and (c) respectively. (d) without blocking layer.

Table I. Photovoltaic performances of the DSSC based on TiO_2 electrodes with different thickness of blocking layers.

Thickness of blocking layer (nm)	Integral photocurrent J_{sc} (mA/cm²)	Open circuit voltage V_{oc} (V)	Fill factor FF	Efficiency η (%)
0	3.60	0.69	0.58	1.45
150	5.14	0.65	0.49	1.63
300	5.80	0.69	0.52	2.07
450	6.10	0.67	0.43	1.75

From Table I it can be seen that though the DSSC devices with the 450 nm thickness of the blocking layer has the highest photocurrent, the maxima conversion efficiency is achieved for DSSC devices with the 300 nm thickness of the blocking layers. This variation can be related to the variations of the fill factor and the open-circuit voltage. The DSSCs with blocking layers show a low fill factor and a low open-circuit voltage, comparing to those without blocking layer. However, the DSSC with 300 nm thickness blocking layer shows the relative high fill factor and open-circuit voltage comparing to DSSCs with 150 nm and 450 nm thickness blocking layers and results in high conversation efficiency.

The fill factor (FF) is defined by

$$FF = \frac{I_{max} V_{max}}{I_{sc} V_{oc}} = \frac{P_{max}}{I_{sc} V_{oc}} \quad (1)$$

where P_{max} is the maximum power generated by solar cell at a voltage V_{max} and current I_{max}; I_{sc} is the short-circuit current and V_{oc} is the open-circuit voltage. The fill factor depends on the shunt resistance R_{sh} which is given by the slope of the tangent line at I_{sc} and the series resistance R_s which is given by the slope of the tangent line at V_{oc}. Both of these resistances are internal, and represent energy dissipation mechanisms in the cell. Ideally, one would like zero series resistance and infinite shunt resistance in order to dissipate the generated power at the external circuit, and then, to maximize the fill factor up to unity. Parallel current paths such as electron back transfer and charge recombination within the device are possible cause of poor fill factor. An ideal cell should offer high internal resistance (shunt resistance) to these parallel currents. Another possible reason for poor fill factor is the high series resistance at the

cell–external circuit junction. High sheet resistance of the ITO plate and/or high resistance at this junction developed during processing of DSC are possible reason for this high series resistance.

From the Figure 5 it can be seen that the introduction of the blocking layer improves the series resistance but worsens the shunt resistance. The DSSCs with different thickness blocking layers have a similar series resistance. The series resistance of dye-sensitized solar cells consists of three resistance elements, namely, sheet resistance of the transparent conducting substrate, resistance of ionic diffusion in the electrolyte, and resistance of the interface between the counter electrode and the electrolyte.[8] It can be seen that the thickness of the blocking layer will not have influences on these resistance as it can be seen in Figure 5 that the DSSCs with different thickness of the blocking layers show the similar series resistance. However, the DSSC with 300 nm thickness blocking layer show a good shunt resistance. That means the variation of the fill factor results from the variation of the shunt resistance. It has been mentioned before that the shunt resistance results from the electron back transfer and charge recombination within the device, the thickness of the blocking layer will have influences on these parameters and results in a difference of the fill factor and then the conversion efficiency.

4. CONCLUSIONS

The different thickness of TiO_2 blocking layers prepared by sputtering technique have been introduced between ITO substrate and sputtered TiO_2 nanorod films. The introduction of these blocking layers does not show a clear influence on TiO_2 nanorod films structure. The photocurrent of the DSSCs has been great improved by introducing the blocking layers. The maximum conversion efficiency (about 2.07%) has been achieved by introducing a 300 nm thickness blocking layer, a 40% improvement comparing to the DSSC without any blocking layer.

References and Notes

1. B. Oregan and M. Gratzel, *Nature* 353/6346, 737 **(1991)**.
2. M. Gratzel, *Journal of Photochemistry and Photobiology C-Photochemistry Reviews* 4/2, 145 **(2003)**.
3. H. J. Jo, Y. C. Choi, D. K. Lee, S. H. Lee, N. K. Park, T. J. Lee, and J. H. Kim, *Molecular Crystals and Liquid Crystals* 514, 422 **(2009)**.
4. C. Longo and M. A. De Paoli, *J. Braz. Chem. Soc.* 14/6, 889 **(2003)**.
5. K. J. Hwang, J. W. Lee, H. S. Yoon, H. D. Jang, J. G. Kim, J. S. Yang, and S. J. Yoo, *Bull. Korean Chem. Soc.* 30/10, 2365 **(2009)**.
6. B. Liu and E. S. Aydil, *J. Am. Chem. Soc.* 131/11, 3985 **(2009)**.
7. S. Nakade, M. Matsuda, S. Kambe, Y. Saito, T. Kitamura, T. Sakata, Y. Wada, H. Mori, and S. Yanagida, *J. Phys. Chem. B* 106/39, 10004 **(2002)**.
8. Y. Chiba, A. Islam, R. Komiya, N. Koide, and L. Y. Han, *Appl. Phys. Lett.* 88/22, 223505 **(2006)**.
9. M. M. Gomez, N. Beermann, J. Lu, E. Olsson, A. Hagfeldt, G. A. Niklasson, and C. G. Granqvist, *Solar Energy Materials and Solar Cells* 76/1, 37 **(2003)**.
10. M. F. Hossain, S. Biswas, T. Takahashi, Y. Kubota, and A. Fujishima, *Thin Solid Films* 516/20, 7149 **(2008)**.
11. S. H. Kang, M. S. Kang, H. S. Kim, J. Y. Kim, Y. H. Chung, W. H. Smyri, and Y. E. Sung, *J. Power Sources* 184/1, 331 **(2008)**.
12. Y. M. Sung and H. J. Kim, *Thin Solid Films* 515/12, 4996 **(2007)**.
13. S. H. Kang, J. W. Lim, H. S. Kim, J. Y. Kim, Y. H. Chung, and Y. E. Sung, *Chem. Mater.* 21/13, 2777 **(2009)**.
14. R. Hattori and H. Goto, *Thin Solid Films* 515/20-21, 8045 **(2007)**.
15. J. N. Hart, D. Menzies, Y. B. Cheng, G. P. Simon, and L. Spiccia, *Comptes Rendus Chimie* 9/5-6, 622 **(2006)**.
16. B. Yoo, K. J. Kim, S. Y. Bang, M. J. Ko, K. Kim, and N. G. Park, *J. Electroanal. Chem.* 638/1, 161 **(2010)**.
17. M. Wu, Z. H. Yang, Y. H. Jiang, J. J. Zhang, S. Q. Liu, and Y. M. Sun, *J. Solid State Electrochem.* 14/5, 857 **(2010)**.
18. J. Y. Kim, S. Lee, J. H. Noh, H. S. Jung, and K. S. Hong, *J. Electroceram.* 23/2-4, 422 **(2009)**.
19. M. H. Kim and Y. U. Kwon, *J. Phys. Chem. C* 113/39, 17176 **(2009)**.
20. S. Lee, J. H. Noh, H. S. Han, D. K. Yim, D. H. Kim, J. K. Lee, J. Y. Kim, H. S. Jung, and K. S. Hong, *J. Phys. Chem. C* 113/16, 6878 **(2009)**.
21. S. M. Waita, B. O. Aduda, J. M. Mwabora, G. A. Niklasson, C. G. Granqvist, and G. Boschloo, *J. Electroanal. Chem.* 637/1-2, 79 **(2009)**.
22. J. K. Lee, B. H. Jeong, S. I. Jang, Y. S. Yeo, S. H. Park, J. U. Kim, Y. G. Kim, Y. W. Jang, and M. R. Kim, *Journal of Materials Science-Materials in Electronics* 20, 446 **(2009)**.
23. L. J. Meng, T. Ren, and C. Li, *Appl. Surf. Sci.* 256/11, 3676 **(2010)**.
24. Y. Zhao, C. Z. Li, X. H. Liu, F. Gu, H. B. Jiang, W. Shao, L. Zhang, and Y. He, *Mater. Lett.* 61, 79 **(2007)**.
25. G. K. Mor, O. K. Varghese, M. Paulose, K. Shankar, and C. A. Grimes, *Sol. Energy Mater. Sol. Cells* 90/14, 2011 **(2006)**.
26. H. C. Ong, A. X. E. Zhu, and G. T. Du, *Appl. Phys. Lett.* 80/6, 941 **(2002)**.
27. L. J. Meng and M. P. Santos, *Mat. Res. Soc. Proc.* 436, 523 **(1997)**.

Received: 20 July 2010. Accepted: 20 November 2010.